ENSO's Phase Locking to the Seasonal Cycle in the Fast-SST, Fast-Wave, and Mixed-Mode Regimes

ELI GALANTI AND ELI TZIPERMAN

Department of Environmental Sciences, The Weizmann Institute of Science, Rehovot, Israel

(Manuscript received 21 September 1998, in final form 14 June 1999)

ABSTRACT

The physical mechanism underlying ENSO's phase locking to the seasonal cycle is examined in three parameter regimes: the fast-SST limit, the fast-wave limit, and the mixed SST–wave dynamics regime. The seasonal cycle is imposed on simple ordinary differential equation models for each physical regime either as a seasonal ocean–atmosphere coupling strength obtained from the model of Zebiak and Cane or as a climatological seasonal upwelling. In all three parameter regimes, the seasonal variations in the ocean–atmosphere coupling strength force the events to peak toward the end of the calendar year, whereas the effect of upwelling is shown to be less important. The phase locking mechanism in the mixed-mode and fast-SST regimes relies on the seasonal excitation of the Kelvin and the Rossby waves by wind stress anomalies in the central Pacific basin. The peak time of the events is set by the dynamics to allow a balance between the warming and cooling trends due to downwelling Kelvin and upwelling Rossby waves. This balance is obtained because the warming trend due to the large-amplitude Kelvin waves, amplified by a weak Northern Hemisphere wintertime ocean–atmosphere coupling strength, balances the cooling trend due to weak Rossby waves, amplified by a strong summertime coupling strength. The difference between the locking mechanisms in the mixed-mode regime and in the fast-SST regime is used to understand the effect of the SST adjustment time on the timing of the phase locking. Finally, in the less realistic fast-wave regime, a different physical mechanism for ENSO's phase locking is revealed through the SST adjustment time and the interaction between the east Pacific region and the central Pacific region.

1. Introduction

One of the predominant characteristics of ENSO is its tendency to peak toward the end of the calendar year (Rasmusson and Carpenter 1982). The east Pacific basinwide warming anomaly (with respect to the monthly mean state) in most recorded events reaches its maximum with in the months November–January [see Fig. 1 of Tziperman et al. (1998), hereafter T98]. Philander (1983) suggested that the key element in the dynamics of the interaction between El Niño and the seasonal cycle is the seasonal movement of the Pacific intertropical convergence zone and its effect on the atmospheric heating and hence on the coupled ocean–atmosphere instability. Other seasonal climatological factors that might enhance the coupled ocean–atmosphere instability possibly leading to ENSO events are large zonal gradients of mean SST, shallow thermocline, strong zonal winds, high SST (Hirst 1986), and strong upwelling (Battisti 1988). Battisti and Hirst (1989) found that setting the basic state in a simplified model to different monthly climatologies affects the rate of anomaly growth. The effects of the above seasonal factors on ENSO's dynamics and phase locking was also attributed to a nonlinear resonance between a nonlinear ENSO oscillator and the periodic seasonal forcing (Tziperman et al. 1994; Jin et al. 1994; Tziperman et al. 1995; Chang et al. 1995).

Although the above works point at possible seasonal climatological variables that affect El Niño's development and dynamics, they do not explain the specific physical mechanism by which the seasonal cycle causes El Niño to peak toward the end of the calendar year. Tziperman et al. (1998) examined this mechanism in a heuristic delayed-oscillator model (Suarez and Schopf 1988; Battisti 1988; Cane et al. 1990; Munnich et al. 1991) and suggested that the locking may be explained by a seasonal amplification of Kelvin and Rossby waves by wind stress anomalies in the central Pacific basin. The peak time of the events was proposed to be set by the dynamics to allow a balance between the warming and cooling trends due to downwelling Kelvin and upwelling Rossby waves. This balance is obtained because the warming trend due to the large-amplitude Kelvin waves, amplified by a weak ocean–atmosphere coupling

Corresponding author address: Dr. Eli Galanti, Dept. of Environmental Sciences, The Weizmann Institute of Science, Rohovot 76100, Israel.
E-mail: eli.galanti@weizmann.ac.il

in boreal winter, balances the cooling trend due to weak Rossby waves, amplified by a strong boreal summertime coupling. However, while heuristic idealized models such as that of T98 can be quite illuminating, it is both necessary and possible to use more rigorously derived idealized models at different parameter regimes that are still simple enough to allow exploration of the physical mechanisms of ENSO's phase locking.

Various such idealized models have been used to examine ENSO's dynamics in the absence of the seasonal cycle. Neelin (1991), Jin and Neelin (1993a), Neelin and Jin (1993), and Jin and Neelin (1993b) (hereafter JN93) defined three parameter regimes for ENSO's dynamics (see also Neelin et al. 1998): the fast-SST regime in which the response of the SST to thermocline depth changes is instantaneous; the fast-wave limit in which the speed of ocean waves (Kelvin and Rossby) is taken to be infinite, that is, instantaneous adjustment of the thermocline to wind stress anomalies (Neelin 1991; Hao et al. 1993); and the mixed-mode regime in which both SST response time and oceanic wave propagation are important (Jin 1997a,b). Other ENSO paradigms focus on different oceanic characteristics and processes such as the displacement of the Pacific warm pool and zonal advection of SST (Picaut et al. 1997), or the role of the Hadley and Walker circulations in the formation of a stationary SST mode (Li 1997).

In this work, we investigate the interaction between ENSO-like oscillations and the seasonal cycle using several idealized, yet carefully derived, models. The models are all based on the dynamics and thermodynamics of the coupled ocean–atmosphere model of Zebiak and Cane (1987) (hereafter CZ model). We consider seasonal variations in the strength of the response of the wind stress anomalies to SST anomalies, which—at least in the framework of Zebiak and Cane (1987)—is sensitive to the mean wind convergence and mean SST (Tziperman et al. 1997). Both the mean atmospheric convergence and mean SST determine the strength of the CZ model atmospheric heating due to a given SST anomaly, and thus determine the strength of the wind stress anomalies (Zebiak and Cane 1987). Thus, the same SST anomaly can result in different wind stress anomalies in different months due to the variation of the climatological SST and wind convergence from month to month. We also consider the role of the seasonal variations in the mean upwelling in ENSO's phase locking. The phase locking of ENSO events is analyzed in the fast-SST limit, fast-wave limit, and the mixed-mode regime (JN93). Simplified ordinary differential equation (ODE) models are derived for each regime, and the interaction between El Niño and the seasonal cycle is interpreted in terms of physical processes such as wave propagation, SST adjustment time, etc. While the mixed-mode regime is the more realistic of the three, it will be seen below that investigating the less realistic fast-SST and fast-wave regimes significantly helps in illuminating the role of the different mechanisms acting in the more realistic mixed-mode regime.

Our interpretation of the El Niño's phase locking mechanism for the mixed-mode and fast-SST regimes is, in general, similar to that of T98 but provides a more physical and quantitative picture, revealing the robust, as well as uncertain, aspects of the locking mechanism. In the fast-wave regime, a totally different interpretation of the locking is required, due to the fact that the SST adjustment time, rather than the ocean wave travel time, is the source of the oscillatory ENSO-like behavior.

The paper is organized as follows. In section 2 we derive a simple ODE in the mixed-mode regime, into which the seasonal cycle in introduced. The derivation follows Jin's (1997b) physical assumptions yet uses a different analytical approach, based on integration along wave characteristics. Results are analyzed both for the nonlinear and linear cases, and the physical mechanism for phase locking is presented. In section 3, a model for the fast-SST limit is derived out of the mixed-mode model of the previous section, and the role of SST adjustment time in the locking mechanism is explored. Section 4 is devoted to the fast-wave regime, in which a different ODE model is constructed, following the partial differential equation (PDE) model of Hao et al. (1993). Again, a similar analysis of the phase locking is applied and the phase locking mechanism is explained. In section 5 we analyze the seasonal ocean–atmosphere coupling strength in the CZ model to provide a basis for the seasonal coupling strength used in our idealized models. We conclude in section 6.

2. The mixed-mode regime

a. Model equations

Our mixed SST–wave dynamics model is mostly based on the ''recharge oscillator'' model of Jin (1997a,b), in which model variables are evaluated at an equatorial strip and at an off-equatorial strip, and in which the oceanic basin is divided into two zonal boxes. In Jin (1997a,b), thermodynamics are governed by mean upwelling and thermal damping, and Kelvin waves are filtered from the equations, leaving off-equatorial Rossby waves to determine the ocean dynamics timescale. In contrast, we retain the Kelvin waves and, furthermore, derive the model as a delayed-oscillator equation for SST in the east Pacific. Both oceanic wave timescales and thermodynamic timescales play a role in the model; hence it is in the mixed wave dynamics–SST regime of JN93. Following the two-strip approximation of Jin (1997b), the equations for the ocean dynamics are solved for the equatorial-strip and for the off-equatorial-strip along-wave characteristics.

1) OCEAN DYNAMICS

The model of Jin (1997a,b) is derived from CZ-like ocean dynamics, of a shallow-water anomaly model on an equatorial β plane. Further simplification is achieved by neglecting the meridional damping ($-\epsilon_m v$) and the meridional wind stress ($\tau_y/\rho H$) terms. The resulting set of equations is

$$\frac{\partial u}{\partial t} - \beta y v + g' \frac{\partial h}{\partial x} = -\epsilon_m u + \frac{\tau_x}{\rho H}, \tag{1a}$$

$$\beta y u + g' \frac{\partial h}{\partial y} = 0, \tag{1b}$$

$$\frac{\partial h}{\partial t} + H\left[\frac{\partial u}{\partial x} + \frac{\partial v}{\partial y}\right] = -\epsilon_m h, \tag{1c}$$

where u and v are the zonal and meridional anomaly velocities, h is the thermocline depth departure from its mean state, g' is the reduced gravity acceleration, ϵ_m is the oceanic damping coefficient, and H is the mean thermocline depth.

Eliminating u and v from (1), a single equation for h can be obtained,

$$\beta y^2(\partial_t + \epsilon_m)h + \frac{g'H}{\beta}\left[\frac{2}{y}\partial_y - \partial_{yy}\right](\partial_t + \epsilon_m)h - g'H\partial_x h + \frac{1}{\rho}(\tau_x - y\partial_y\tau_x) = 0. \tag{2}$$

Following Jin (1997b) we wish to evaluate the equation at the equator ($y = 0$), and at a zonal band off the equator ($y = y_n$). This ''two-strip'' approximation assumes that the ocean dynamics in the equatorial region is well represented by a combination of equatorial Kelvin waves and off-equatorial long Rossby waves, both well represented by the two strips at latitudes $y = 0$ and y_n.

A Kelvin wave solution of the form

$$h(x, y, t) = h_e(x, t)\exp\left(-\frac{\beta}{2C_o}y^2\right), \tag{3}$$

where $C_o = \sqrt{g'H}$, satisfies Eq. (2), and therefore, taking advantage of the known meridional structure, we get an equation at $y = 0$ of the form

$$-C_o\partial_x h_e + (\partial_t + \epsilon_m)h_e = \frac{1}{C_o\rho}\tau_{ex}, \tag{4}$$

where τ_{ex} is the wind stress at the equator. In Jin (1997a) the second term on the lhs of (4) is neglected, leaving the east–west thermocline tilt to be in a balance with the wind stress, thus omitting the Kelvin wave propagation. We differ from this strategy by retaining the Kelvin waves. Next, rather than using Jin's (1997a) two-box model along the x axis, we integrate (4) over the trajectory of an eastward propagating Kelvin wave that starts from the western boundary at a time $t - \tau_2$ and reaches the eastern boundary at a time t, where $\tau_2 = L/C_o$ is the Kelvin crossing time of a basin of length L. The wave is assumed to be excited by the wind stress in the central part of the basin, from $x = x_W + 0.25L$ to $x = x_W + 0.75L$. The wind stress is evaluated at the middle of the basin, $x = x_w + L/2$, at a time $t - \tau_2/2$, which is the time when the Kelvin wave crosses the middle of the basin. We denote the thermocline depth anomaly at the western (eastern) edge of the basin by h_{eW} (h_{eE}), and the solution to (4) is then

$$h_{eE}(t) = h_{eW}(t - \tau_2)e^{-\epsilon_m\tau_2} + \frac{1}{\rho C_o}dt\tau_2\tau_{ex}\left(\frac{L}{2}, t - \frac{\tau_2}{2}\right)e^{-\epsilon_m(\tau_2/2)}, \tag{5}$$

where $dt = 0.5$ is the fraction of crossing time during which the wind stress affects the oceanic waves.

Next, we wish to solve (2) at the off-equatorial band ($y = y_n$), in order to include the Rossby wave dynamics in the model. It can be shown that at $y_n \geq 2L_o$ (where L_o is the oceanic Rossby radius of deformation) the second term in (2) is negligible (Jin 1997b), resulting in the off-equatorial equation

$$-\frac{C_o^2}{\beta y_n^2}\partial_x h_n + (\partial_t + \epsilon_m)h_n = \frac{1}{\beta\rho}\left[\frac{\partial}{\partial y}\left(\frac{\tau_x}{y}\right)\right]_{y=y_n}. \tag{6}$$

Solving (6) again along characteristics for a Rossby wave that starts from the eastern boundary at time $t - \tau_1$, where $\tau_1 = Ly_n^2\beta/C_o^2$ is the Rossby crossing time of a basin length L, at a latitude y_n, we find

$$h_{nW}(t) = h_{nE}(t - \tau_1)e^{-\epsilon_m\tau_1} - \frac{1}{\beta\rho}dt\tau_1\left[\frac{\partial}{\partial y}\left(\frac{\tau_x}{y}\right)\right]_{[y_n, L/2, t-(\tau_1/2)]}e^{-\epsilon_m(\tau_1/2)}. \tag{7}$$

The eastern and western boundary conditions represent the reflection of Kelvin waves into Rossby waves at the east, and the reflection of Rossby waves into Kelvin waves at the west. In terms of the thermocline depth at the boundaries, these boundary conditions are

$$h_{eW} = r_W h_{nW}, \qquad h_{nE} = r_E h_{eE}, \tag{8}$$

where r_W and r_E are reflection coefficients at the western and eastern boundaries, respectively. Using the above boundary conditions, (5) and (7) may be joined to give an expression for the equatorial thermocline depth anomaly at the eastern Pacific,

$$h_{eE}(t) = e^{-\epsilon_m\tau_2}r_W\left[r_E h_{eE}(t - \tau_1 - \tau_2)e^{-\epsilon_m\tau_1} - \frac{1}{\beta\rho}dt\tau_1\left[\frac{\partial}{\partial y}\left(\frac{\tau_x}{y}\right)\right|_{[y_n,L/2,t-\tau_2-(\tau_1/2)]}\right]e^{-\epsilon_m(\tau_1/2)}\right]$$
$$+ \frac{1}{\rho C_o}dt\tau_2\tau_{ex}\left(\frac{L}{2}, t - \frac{\tau_2}{2}\right)e^{-\epsilon_m(\tau_2/2)}. \quad (9)$$

This form of equation manifests clearly the delayed dependence of $h_{eE}(t)$ on the wave dynamics. The first term represents the Rossby wave that left the eastern boundary at a time $t - \tau_1 - \tau_2$, was reflected as a Kelvin wave at time $t - \tau_2$, and arrived in the eastern Pacific at time t. The second term represents the Rossby waves excited at a time $t - \tau_2 - \tau_1/2$ in the central Pacific, and the third represents the Kelvin waves excited at a time $t - \tau_2/2$. Note that while T98 described the influence of the wind stress on the ocean dynamics as *amplification* of the Kelvin and Rossby waves, the above more rigorously derived equations indicate that a more appropriate description is that the wind stress *excites* new such waves rather than amplify existing ones.

2) THERMODYNAMICS

The equation describing SST changes at the equator is based on that of Zebiak and Cane (1987). Following Jin (1997a), we only keep the time rate of change, the advection by the mean upwelling $\overline{w}$, and the damping terms,

$$\partial_t T = -\epsilon_T T - \gamma\frac{\overline{w}}{H_1}(T - T_{\text{sub}}(h)), \quad (10)$$

where ϵ_T is a thermal damping coefficient, and $T_{\text{sub}}(h)$ is the temperature anomaly at a depth H_1 and is a function of the thermocline depth anomaly h (Munnich et al. 1991; Zebiak and Cane 1987; see appendix A). The parameter γ relates the temperature anomalies entrained into the surface layer to the deeper temperature variations due to $T_{\text{sub}}(h)$ (see Zebiak and Cane 1987).

3) OCEAN–ATMOSPHERE INTERACTION

Following Gill (1980), Hao et al. (1993), and Jin (1997b), we take the wind stress to be a function of the SST at the equator (T_e):

$$\tau_x(x, y, t) = \mu A(T_e, x)\exp\left(-\frac{y^2\alpha}{2L_o^2}\right), \quad (11)$$

where $A(T_e, x)$ is a nonlocal function that relates the equatorial SST to wind stress, and μ serves as a relative coupling coefficient that we allow to change seasonally. The wind stress terms in (9) may thus be expressed as

$$\tau_{ex} = \mu A(T_e, x),$$
$$\partial_y(\tau_x/y)|_{y=y_n} = -\mu A^* A(T_e, x), \quad (12)$$

where

$$A^* = \left[\frac{L_o^2 + \alpha y_n^2}{(y_n L_o)^2}\right]e^{-(y_n^2\alpha/2L_o^2)}, \qquad \alpha = \left(\frac{L_o}{L_a}\right)^2,$$

and L_a is the atmospheric Rossby radius of deformation. Here, $A(T_e, x)$ may be obtained by solving a Gill-type atmospheric model (Gill 1980) using a long-wave approximation (see Hao et al. (1993), or (B1) in appendix B below), resulting in a linear relation between the wind stress and the equatorial SST. As in Jin (1997a), the function $A(T_e, x)$ for the wind stress in the central Pacific, appearing in (9), is now assumed to be proportional to the temperature in the eastern Pacific:

$$A(T_e, x = x_w + L/2) = b_0 T_{eE}(t), \quad (13)$$

where b_0 is the annual mean coupling strength. The assumption embedded in (13) is that most of the SST variability is in the eastern part of the equatorial Pacific. The resulting wind stress, according the Gill model, will be in the central Pacific (Jin 1997a).

4) MIXED-MODE MODEL

Equation (9) can be written, using (13) and (12), as

$$h_{eE}(t) = e^{-\epsilon_m\tau_2}r_W r_E h_{eE}(t - \tau_1 - \tau_2)e^{-\epsilon_m\tau_1}$$
$$- e^{-\epsilon_m\tau_2}r_W\frac{1}{\beta\rho}A^* dt\tau_1\mu\left(t - \tau_2 - \frac{\tau_1}{2}\right)$$
$$\times b_0 T_{eE}\left(t - \tau_2 - \frac{\tau_1}{2}\right)e^{-\epsilon_m(\tau_1/2)}$$
$$+ \frac{1}{\rho C_o}dt\tau_2\mu\left(t - \frac{\tau_2}{2}\right)b_0 T_{eE}\left(t - \frac{\tau_2}{2}\right)e^{-\epsilon_m(\tau_2/2)}, \quad (14)$$

expressing $h_{eE}(t)$ as a function of h_{eE} and T_{eE} at previous times. As before, the first term represents the free Rossby and Kelvin waves, the second represents the excited Rossby wave, and the third represents the excited Kelvin wave. The thermodynamic equation (10) evaluated at the eastern side of the basin gives the dynamical equation in which $h_{eE}(t)$ is used:

TABLE 1. Summary of parameters in the mixed-mode model.

Parameter	Value
Mixed-mode regime	
ϵ_T	4 month^{-1}
γ	0.75
$\overline{w}$	45 m month^{-1}
H_1	75 m
ϵ_m	30 month^{-1}
C_o	2.7 m s^{-1}
L	1.5×10^7 m
L_o	3.4×10^5 m
α	0.1
y_n	6.8×10^5 m
β	2.3×10^{-11} m^{-1} s^{-1}
ρ	1000 kg m^{-3}
τ_1	2.1 month
τ_2	8.5 month
b_0	1.2×10^{-2} kg s^{-2} m^{-1} °C^{-1}
r_W	0.75
r_E	0.9

$$\partial_t T_{eE} = -\epsilon_T T_{eE} - \gamma \frac{\overline{w}}{H_1}(T_{eE} - T_{\text{sub}}(h_{eE})). \quad (15)$$

Equations (14) and (15), together with appendix A for T_{sub}, form our mixed-mode model for the investigation of ENSO's tendency to peak toward the end of the calendar year. Hereafter we denote T_{eE} by T and h_{eE} by h. Note that the nonlinearity in the model is due to the nonlinear function $T_{\text{sub}}(h)$.

b. Results

The mixed-mode delayed oscillator model [(14), (15)] was solved numerically using the Numerical Algorithm Group routine D02CBF (Numerical Algorithm Group 1984). The values of all model parameters are specified in Table 1. In the absence of a seasonal cycle, model integration shows similar results to that of Jin (1997a). Events occur every 4.3 yr with an averaged maximum of east Pacific warming amplitude around 2.5°C (not shown). As expected, there is no phase locking to the seasonal cycle as the latter is not represented in the model. In the next section, we impose on the model a seasonally varying relation between the wind stress and the SST, as well as a seasonally varying climatological upwelling, and analyze their interaction with the ENSO-like oscillations.

1) SEASONALLY VARYING OCEAN–ATMOSPHERE COUPLING STRENGTH

The seasonal cycle may enter in our model via two different physical mechanisms. The first and most important is the ocean–atmosphere seasonal coupling coefficient μ in (14). The seasonal variation in this parameter was shown to be, at least in the CZ model, a result of the seasonal cycle in both the mean SST and wind divergence (Tziperman et al. 1997). The influence

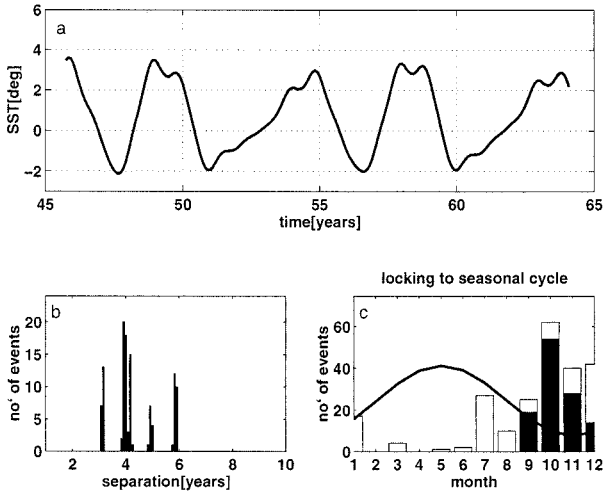

FIG. 1. The effect of a seasonally varying coupling strength in the mixed-mode model equations (14) and (15): (a) a time series of the model eastern Pacific temperature; (b) histogram of the separation between events; (c) number of event peaks in each month of the calendar year (black bars are for El Niño events and white bars are for La Niña events).

of the mean SST and mean wind convergence on ocean–atmosphere interaction is through their effect on the atmospheric heating (Philander 1983; Hirst 1986; Tziperman et al. 1997). The other parameter that may vary seasonally is the mean upwelling ($\overline{w}$) in the eastern equatorial Pacific appearing in the SST equation.

For simplicity we take the relative coupling coefficient to vary in time as a cosine with a 1-yr period. The phase is taken to be such that maximum coupling is reached in the middle of May and its minimum value in the middle of November,

$$\mu = 1 + \varepsilon \cos(w_a t - \phi), \quad (16)$$

where ε is the strength of the seasonal cycle (taken to be 0.1), $w_a = 2\pi/12$ is the annual frequency, and $\phi = 5\pi/6$ is the phase. We base the seasonal variations in the coupling strength on the analysis of the CZ model presented below in section 5, showing that the coupling strength reaches its maximum in May and its minimum in September.

Figures 1a–c show the results for this case. The SST time series in Fig. 1a shows that events are not as regular as in the absence of a seasonal cycle (see Tziperman et al. 1994; Jin et al. 1994; Tziperman et al. 1995; Chang et al. 1995). Their amplitude now varies from 2° to 4°C; event occurrence is every 3–6 yr (Fig. 1b); and the most pronounced finding, shown in Fig. 1c, is that events tend to peak in the months September–December, about 6 months after the coupling maximum strength, and when the coupling is reaching its minimum. This finding is in agreement with T98, although the model used here is very different.

Sensitivity tests show that the model displays ENSO-like variability in a parameter regime that is within about

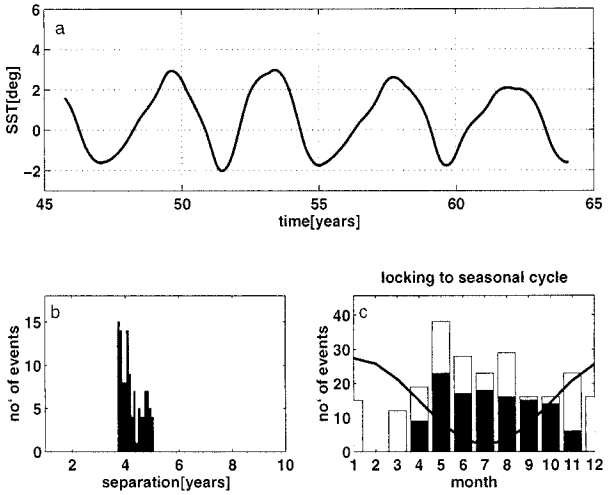

FIG. 2. As in Fig. 1, for seasonal upwelling.

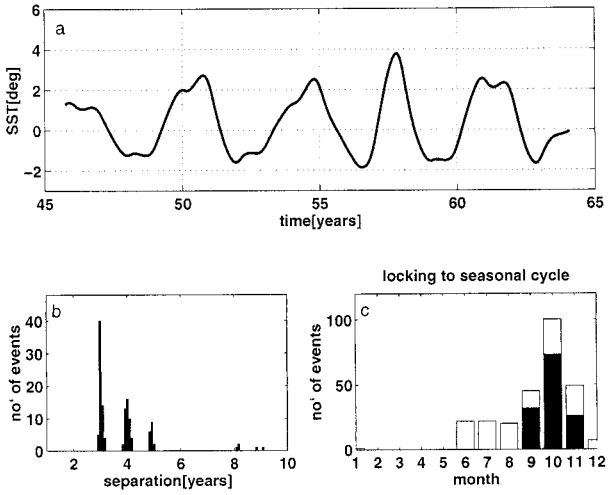

FIG. 3. As in Fig. 1, for the combined case of seasonal coupling strength and seasonal upwelling.

10% of the model parameters specified in Table 1, with individual parameter sensitivity that allows for ENSO-like variability being from 5% to 20%. In any case, within the ENSO-like regime, the model phase locking is very robust; that is, its tendency to peak toward the end of the calendar year persists even when the event's amplitude or frequency changes when model parameters are perturbed.

2) SEASONALLY VARYING UPWELLING

The influence of a seasonally varying upwelling was investigated by Tziperman et al. (1997) using the CZ model. Their two main findings were that seasonal upwelling variations are of a second-order significance to ENSO's locking to the seasonal cycle, and that in the absence of seasonal upwelling variations, the event amplitude rises fairly significantly.

In our model, mean upwelling is a key parameter; changing its value influences the model behavior substantially. For instance, increasing its value by 20% causes events to be stronger (about 4° at the peak) and less regular, and the separation between events shortens from 4 to 3 years. A similar decrease in upwelling will affect the model in the opposite way.

The climatological seasonal upwelling used in the CZ model varies in the east equatorial Pacific from around 60 m month^{-1} in January to around 30 m month^{-1} in June. We therefore take the climatological upwelling to be $\overline{w}[1 + 0.25\cos(2\pi t/12)]$, where $t = 0$ coincides with the beginning of January. In the run shown in Fig. 2, ocean–atmosphere coupling is set to its annual mean value, leaving only the upwelling to vary seasonally. In this case, events tend to peak in May–October when the upwelling reaches its minimum, and more significantly, the event peaks are less locked to the seasonal cycle than in the seasonally varying coupling strength case.

3) COMBINED EFFECT OF COUPLING STRENGTH AND UPWELLING

Next we wish to examine the event locking to the seasonal cycle when both the ocean–atmosphere coupling and the mean upwelling change seasonally (Fig. 3). In spite of the seasonally varying upwelling, the event's peak time remains confined to September–November, almost as in the case of seasonally varying coupling strength only (see Fig. 1). This result, together with those of Fig. 2, implies that the overall influence of upwelling is of a secondary importance in comparison with the influence of the ocean–atmosphere coupling coefficient (i.e., the influence of climatological seasonal SST and wind divergence). Another finding is that the averaged El Niño amplitude is now smaller than that of the standard case. Both findings are in a striking agreement with the experiments of Tziperman et al. (1997) using the fuller CZ model, suggesting that the simplified model captures the essence of the CZ model.

In all three runs of the model presented above, the phase locking of the weaker La Niña events is less robust than that of the El Niño events. This less robust locking is a result of the asymmetry in the function $T_{\text{sub}}(h)$, which results in a weaker feedback between thermocline movements and SST during La Niña events. This weaker feedback is also the reason for the La Niña events being weaker than the El Niño events. The phase locking of observed La Niña events to the seasonal cycle is, like in our model, less robust than that of the El Niño events, and we will therefore address in the following only to the phase locking of El Niño events.

c. Physical mechanism for phase locking in the mixed-mode regime

We now derive a linearized version of the model, in order to analyze the mechanism that controls El Niño's

locking to the seasonal cycle in the mixed-mode regime. The linearization of the model allows us to separate the different processes (Rossby and Kelvin waves, and upwelling) that affect the SST in the eastern equatorial Pacific and to carefully analyze each term in a way that is not possible with the nonlinear model. It is shown below that this linearization does not affect the nature of the oscillations and its phase locking. Expanding T_{sub} in a Taylor series, with only the first term retained, we find

$$T_{\text{sub}} \cong \delta h, \tag{17}$$

where $\delta \equiv \partial_h T_{\text{sub}}|_{h=0} = 0.25$ [°C m^{-1}].

The solution of this linearized model is shown in Figs. 4a–c. It is very convenient to analyze the physical mechanism when the oscillations are exactly neutrally stable in between these two regimes, which occurs for $b_0 = 1.476 \times 10^{-2}$. This tuning of b_0 is needed because without the nonlinearity, which limits the event amplitude, the linearized model can produce either exponentially growing or exponentially decaying oscillation. Events are still locked to the end of the year as in the nonlinear model, and therefore analyzing the linear model should reveal the physical mechanism of the nonlinear model as well.

In the fully nonlinear model, nonlinear phase locking to the external periodic seasonal forcing can drive different initial conditions to the same phase locked solution. In the linearized model, however, the phase information of the initial conditions is preserved during the model run. We therefore need to show that the phase locking in the linearized model does not depend on the initial conditions. Figure 5 shows 12 superimposed SST time segments from the linear model, each corresponding to an integration that is initialized in the same way, yet at a different month. In spite of the fact that each integration has a different initial phase with respect to the seasonal cycle, events in all integrations reach their peaks at the end of the year. Therefore, ENSO's phase locking in our simple model is not a result of its nonlinearity but is a result of the seasonal modulation of the background model parameters. This behavior was also found by Battisti and Hirst (1989) in their simplified models. We can now proceed to understand the details of the physical locking mechanism in the linear model, with the understanding that it also applies to the nonlinear model for which the separation of terms cannot be done explicitly.

Substituting (17) in (15) results in

$$\partial_t T = -\epsilon_T T - \gamma \frac{\overline{w}}{H_1}(T - \delta h), \tag{18}$$

where h is evaluated using (14). Time series of all terms (during a specific event) in (18) are shown in Fig. 6. The terms represent

$$\text{DO} = -\epsilon_T T \tag{19}$$

$$\text{DU} = -\gamma \frac{\overline{w}}{H_1} T \tag{20}$$

$$\text{RK} = +\delta\gamma \frac{\overline{w}}{H_1} e^{-\epsilon_m \tau_2} r_W r_E h(t - \tau_1 - \tau_2) e^{-\epsilon_m \tau_1} \tag{21}$$

$$\text{ER} = -\delta\gamma \frac{\overline{w}}{H_1} e^{-\epsilon_m \tau_2} r_W \frac{1}{\beta\rho} A^* dt \tau_1 \mu\left(t - \tau_2 - \frac{\tau_1}{2}\right) \times b_0 T\left(t - \tau_2 - \frac{\tau_1}{2}\right) e^{-\epsilon_m(\tau_1/2)} \tag{22}$$

$$\text{EK} = +\delta\gamma \frac{\overline{w}}{H_1} \frac{1}{\rho C_o} dt \tau_2 \mu\left(t - \frac{\tau_2}{2}\right) \times b_0 T\left(t - \frac{\tau_2}{2}\right) e^{-\epsilon_m(\tau_2/2)}, \tag{23}$$

so that

$$\delta h = \text{RK} + \text{ER} + \text{EK}. \tag{24}$$

The term DO is the thermal damping of the SST; DU is the part of the upwelling that depends on the SST. The first two terms depend on $T(t)$ with a negative coefficient; hence they always tend to diminish SST anomalies. The term RK represents the free Rossby wave that left the eastern boundary of the basin 10 months ($\tau_1 + \tau_2$) before peak time, traveled to the western boundary for about 8 months, and was reflected back as a Kelvin wave that reached the eastern boundary after 2 more months. The emanated wave was damped on its way due to oceanic momentum damping (ϵ_m) and due to imperfect reflection at the western boundary (r_W). The term RK depends only on $h(t - \tau_1 - \tau_2)$ and therefore is not influenced by the seasonal cycle. The term ER stands for the excitation of Rossby waves in the center of the basin due to the wind stress. The excitation is opposite in sign to the wind stress, since positive wind stress (westerlies) causes the shift of warm water toward the equator, thus exciting cold anomalies off the equator that travel westward as upwelling Rossby waves. This is the term that eventually terminates the events, or in other words, this term represents the system's ''memory'' that maintains the oscillation. The fifth term, EK, represents the excitation of Kelvin waves in the mid-Pacific basin, again due to the wind stress, only this time the excitation has the same sign as the wind stress. As before, a positive wind stress anomaly causes warm water to shift from off-equator toward the equator; the warm water excess at the equator drives a thermocline deepening signal that travels eastward as a Kelvin wave, reaching the eastern boundary after about 1 month. Both ER and EK depend on the seasonal cycle through the seasonal sensitivity of wind stress anomalies to SST

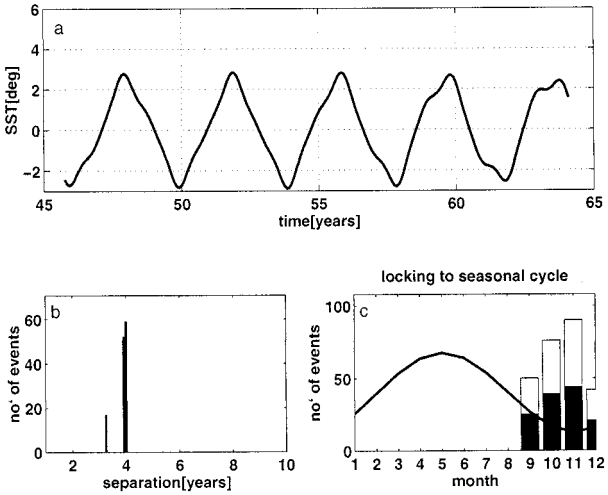

FIG. 4. As in Fig. 1, for the linearized mixed-mode model.

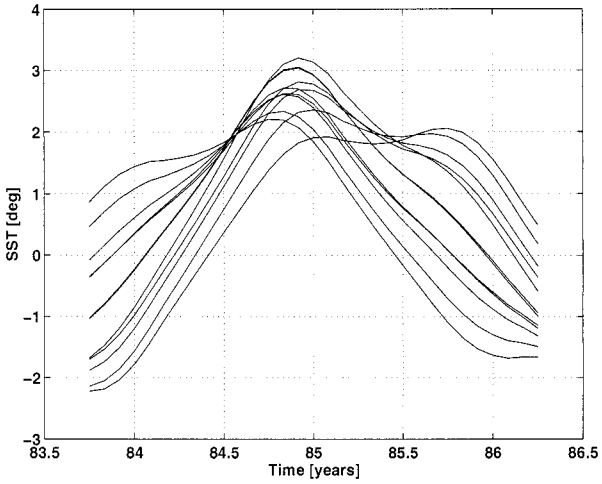

FIG. 5. Twelve time series of SST in the linearized mixed-mode model, corresponding to integrations starting at 12 different months. Events tend to peak toward the end of the calendar year irrespectively of the initial conditions, like in the nonlinear model.

anomalies and therefore are key elements in ENSO's interaction with the seasonal cycle.

Let us now examine the physical mechanism of an event phase locking, examining the different terms in the SST equation (Fig. 6) at the event peak time at $t \approx -0.1$ (i.e., December of year -1; time $t = 0$ is defined to be the 1 January nearest to the event's peak time). At that point all terms at the rhs of (18) cancel each other to give zero temperature time tendency ($\partial T/\partial t = 0$).

The main balance is between the warming Kelvin waves excited in the middle of the basin a month before peak time, EK, and the excited Rossby waves, ER, that cool the SST. The excited Kelvin waves are forced by the large wind stress that existed a month before the event peak time. Yet, these Kelvin waves' amplitude is affected at the time of excitation by the small coupling strength in the boreal winter, near the event peak time [μ in Eq. (19)]. The excited Rossby waves, ER, are forced by the wind anomaly 6 months before their arrival at the eastern boundary as Kelvin waves. At that time, the event amplitude and thus the amplitude of the wind that has forced these waves are small. However, the coupling strength 6 months prior to the event peak time, during boreal spring and early summer, is large, resulting in a significant amplitude of the excited cold Rossby waves. Thus, exactly at the event peak time, the warm Kelvin waves excited by a strong wind stress and weak coupling balance the cold Rossby waves excited by a weaker wind stress but stronger coupling. This balance depends on the timing between the amplitudes of the seasonal coupling strength and of the ENSO event and could not have occurred in summertime. After the peak time, the cold anomalies dominate the SST tendency equation, and eventually terminate the event.

3. The fast-SST limit

The purpose of this section is to understand the role of the SST adjustment time, which was ignored in section 2, in ENSO's phase locking by analyzing a parameter regime in which this timescale is neglected altogether.

a. Model equations

In the fast-SST limit, the SST adjustment time is much shorter than the ocean dynamics adjustment time, or in other words SST is assumed to respond instantaneously to thermocline depth changes (Neelin 1991; JN93). We obtain our model equations for this limit by

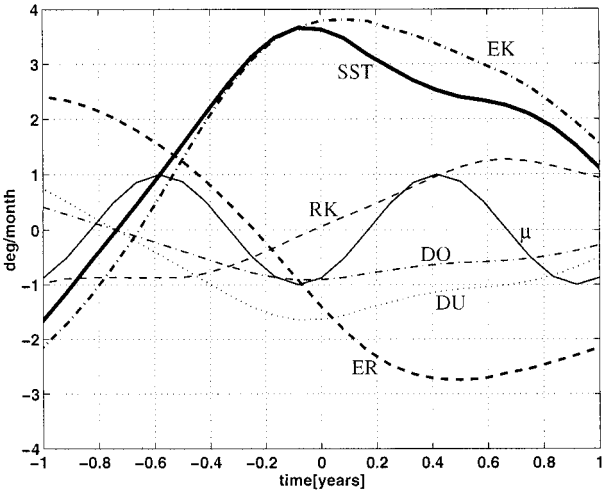

FIG. 6. A time series of the linearized mixed-mode model, showing the terms in the SST tendency equation for one specific event: DO is the thermal damping of the SST; DU is damping due to the upwelling; RK is the free Rossby–Kelvin wave; ER is the excited Rossby wave; and EK is the excited Kelvin wave. The DO, DU, RK, ER, and EK are in °C month^{-1}; SST is in °C. Also shown is the seasonal coupling variation μ.

TABLE 2. Parameters in the fast-SST and fast-wave models, which were modified from the values used in the mixed-mode model.

Parameter	Modified value
Fast-SST limit—version I	
y_n	10×10^5 m
dt	0.75τ
k	0.12 °C m^{-1}
Fast-SST limit—version II	
C_o	2.3 m s^{-1}
dt	0.75τ
k	0.1 °C m^{-1}
Fast-wave limit	
ϵ_a	2.5
x_0	0.75 L
x_c	0.5 L
x_e	0.9 L
b_0	9×10^{-2} kg s^{-2} m^{-1} °C^{-1}

taking the term $\partial_t T_{eE}$ in (15) to be zero, so that the SST equation becomes a diagnostic equation of the form

$$T(t) = \gamma \frac{\overline{w}}{H_1}\left(\epsilon_T + \gamma \frac{\overline{w}}{H_1}\right)^{-1} T_{\text{sub}}(t). \tag{25}$$

Furthermore, instead of using (14) to represent the Rossby and Kelvin waves through integration along wave characteristics, we use (5) for the Kelvin waves, and the prognostic equation (6), discretized using two zonal boxes (Jin 1997a) for Rossby waves,

$$\partial_t h_{nW}(t) = -\epsilon_m h_{nW}(t) + \frac{c^2}{\beta y_n^2 L}(h_{nE}(t) - h_{nW}(t)) - \frac{1}{\beta\rho} A^* \mu(t) b_0 T(t). \tag{26}$$

The reason for this change is to avoid numerical noise that arises in nondifferential delayed equations such as (14), although in principle we could have used (14) and (25).

To obtain an oscillation that resembles the observed ENSO characteristics, some model parameters need to be modified, and since the fast SST limit is not a realistic one, the required change in parameters may lead to less realistic values. We therefore investigated two versions of this limit, both of which simulate reasonable ENSO-like events, but each controlled by a different set of parameters (Table 2). Even though the two versions differ fairly substantially, they display similar locking to the seasonal cycle with a similar locking mechanism, which clearly testifies to the robustness of the phase locking mechanism. As the results are similar for both versions of the fast-SST model, we analyze here version I only.

b. Results

The model was integrated numerically with a seasonally varying coupling coefficient (16), for a period of 500 yr. Figure 7 shows the results for version I: Events show a clear tendency to lock to months August–October with maximum number of event peaks in September. In the mixed-mode regime (Fig. 1), locking to the seasonal cycle was in general similar but shifted by 1–2 months toward the end of the year. The results for version II are similar (not shown) except for the events being stronger and the La Niña events being less locked to the seasonal cycle.

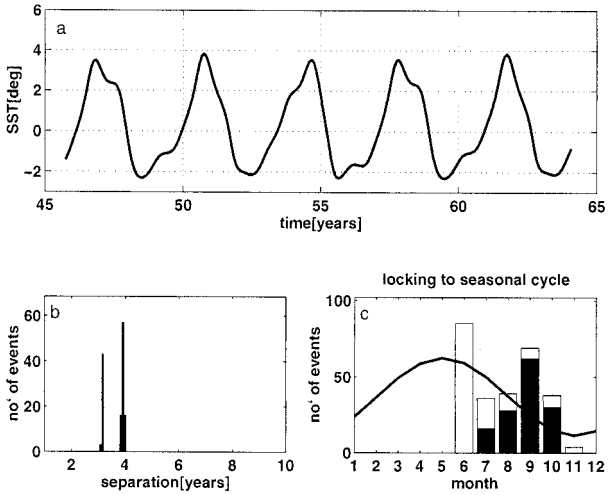

FIG. 7. As in Fig. 1, for the effect of a seasonally varying coupling strength in the fast-SST limit (version I).

c. Phase locking mechanism

In the fast-SST limit, the time of maximum SST anomaly is also a time of maximum thermocline depth anomaly (25). Therefore we can use Eq. (5) for the thermocline depth at the eastern boundary, h_{eE}, in order to analyze the locking of the peak time for both h_{eE} and the SST. The two terms in (5) represent the reflected Rossby wave (ROS), and the Kelvin wave excitation due to wind stress (KEL). In the fast-SST regime, these terms directly determine the SST, whereas in the mixed-mode regime they influence the time derivative of the SST equation along with other factors. For reference we note that ROS in this case is equivalent to the sum of RK and ER in the mixed-mode model; KEL is equivalent to EK. Figure 8 shows time series of all terms for a single event.

While the details of this fast-wave model are different from those of the mixed-mode model of the previous section, the physical mechanism of ENSO's phase locking to the seasonal cycle is still largely the wave dynamics mechanism explained in the previous section, with the related wave timescales (τ_1 and τ_2). The two main competing feedbacks are still the warming Kelvin waves and the cooling Rossby waves. SST maximum is reached when the SST warming tendency due to the Rossby wave excited 6 months prior to the peak time

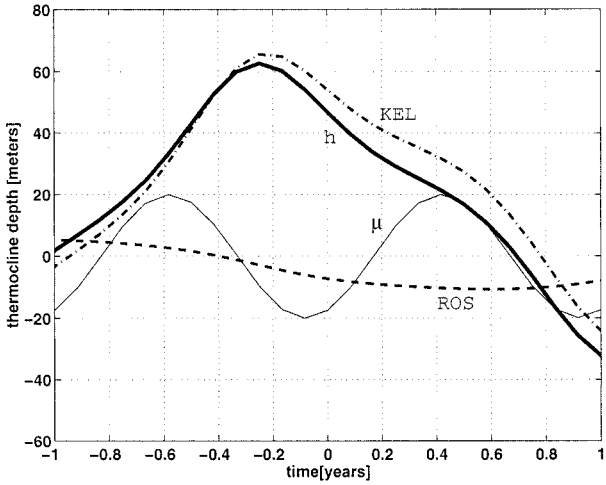

FIG. 8. Time series of the fast-SST limit (version I), showing the terms in the thermocline depth equation for one specific event. KEL is the excited Kelvin wave and ROS is the Rossby wave term.

(ROS term) balances the SST cooling tendency due to the Kelvin excited 1 month prior to the peak time (the KEL term).

However, a comparison between the mixed-mode results (Fig. 1) and the fast-SST results (Fig. 7) shows that there is about 2 months' difference in the event peak time. This 2 months' difference between the mixed-mode regime and the fast-SST limit can be explained by the lack of 2 months' delay time due to upwelling in the fast-SST limit, as $[\overline{w}/H_1]^{-1} \approx 2$ months (25). Therefore, in the mixed-mode regime we can expect events to reach to their maximum 2 months later than events in the fast-SST limit (Fig. 9).

We can therefore conclude this analysis of the fast-SST limit with the main lesson being that the role of the SST adjustment time in the more realistic mixed-mode regime is to shift the peak time by about 2 months toward the end of the calendar year.

4. The fast-wave limit

In the fast-wave limit, the Rossby and Kelvin wave propagation speeds are assumed infinite, resulting in an instantaneous adjustment of ocean thermocline depth and current velocities to wind stress anomalies (Neelin 1991; Hao et al. 1993). Hence, the SST adjustment time to thermocline depth changes plays the central role in the physical mechanism of the oscillations obtained in this parameter regime (Hao et al. 1993). The fast-wave limit results in somewhat unrealistic oscillations, in comparison to both ENSO's timescale and amplitude (JN93; Neelin 1991; Hao et al. 1993), as this is not a realistic ENSO regime. Nevertheless, it is still useful to analyze ENSO's phase locking in this regime, since it reveals some new aspects not considered in the previous two regimes.

a. Model equations

The fast-wave limit can be derived by taking the time derivative terms in the ocean momentum equation (1) to be zero. In the fast-wave limit, the dynamics crucially depend on the east–west tilt of the thermocline. Therefore, we divided the basin into two boxes, one for the east Pacific and one for the central Pacific. The full derivation of the model equations is given in appendix B and is a simplification into a system of ODEs based

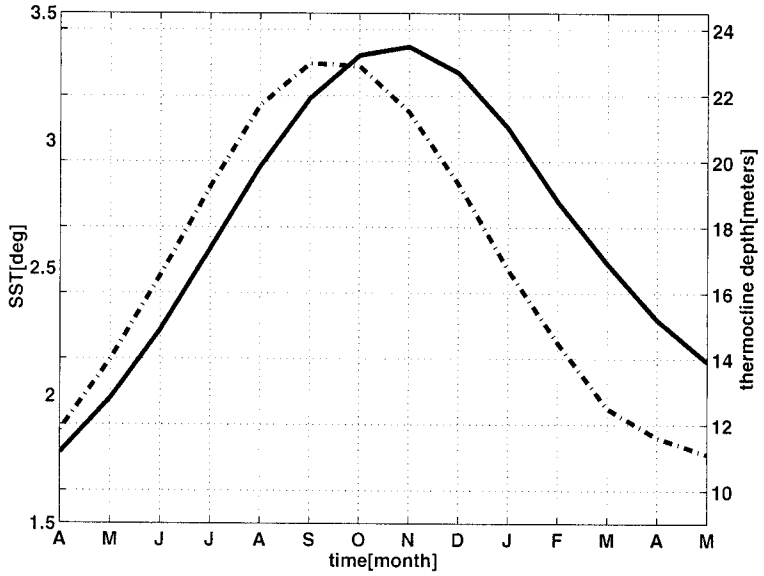

FIG. 9. Time series of SST (solid) and *h* (dash-dot) in the mixed-mode regime. The figure shows the delay between the two, which is missing in the fast-SST regime, causing the locking of events to occur about 2 months earlier in the fast-SST regime.

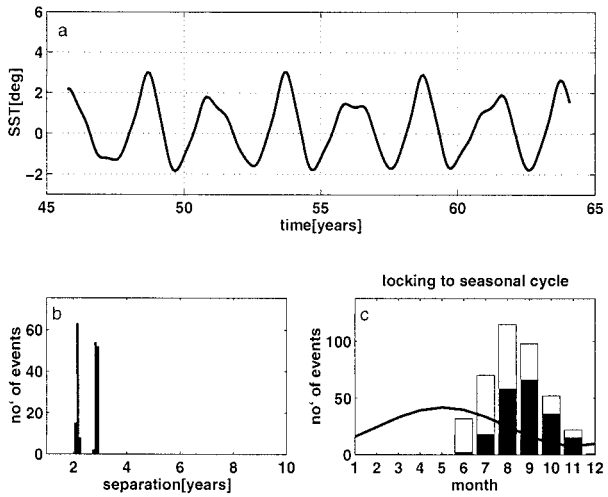

FIG. 10. As in Fig. 1, for a seasonally varying ocean–atmosphere coupling strength in the fast-wave limit.

on the PDE model of Hao et al. (1993). The two SST tendency equations for the two regions are

$$\partial_t T_c = -\epsilon_T T_c - \gamma \frac{\overline{w}}{H_1} T_c + \gamma \frac{\overline{w}}{H_1} T_{\text{sub}}(h_c(T_c, T_e)), \quad (27)$$

$$\partial_t T_e = -\epsilon_T T_e - \gamma \frac{\overline{w}}{H_1} T_e + \gamma \frac{\overline{w}}{H_1} T_{\text{sub}}(h_e(T_c, T_e)), \quad (28)$$

where T_c and T_e are the SST in the central Pacific and the eastern Pacific, respectively; and the dependence of T_{sub} on T_c and T_e is via the thermocline depth anomalies h_c and h_e (see appendix B). Table 2 summarizes the model parameters used for this model.

b. Results

The oscillatory mechanism of the eastward propagating fast-wave oscillations is explained in Hao et al. (1993) (see also appendix B). The seasonal cycle is introduced as before (16) via a coupling coefficient between wind stress and SST anomalies. The simplification in the ocean dynamics and the simple two-box zonal discretization allows us to include a somewhat more elaborated atmospheric model with local ocean–atmosphere coupling in both the eastern and central Pacific. We take here the coupling coefficient to vary seasonally only in the eastern box ($\mu_2 = \mu$), whereas in the central box it remains constant ($\mu_1 = \text{const}$). Events in this seasonal fast-wave model tend to peak in August–October (Fig. 10). Integrating the model with a seasonally varying coupling strength in both boxes shows a weak locking to months May–October (not shown), whereas integration with seasonal coupling in the central basin only results in event peaking in February–June (not shown). Introducing a climatological seasonal upwelling (16) results, as in the mixed-mode regime, in a weak locking to months January–July (not shown). The combined effect of both the seasonal varying coupling coefficient and seasonal upwelling tends to weaken events locking with the maximum event during July–November (not shown). Clearly the phase locking in this regime is not very robust.

c. Physical mechanism for phase locking

Although our model is formulated to be similar to the eastward propagating fast-wave case of Hao et al. (1993), our coarse two-box discretization in the zonal direction eliminates the specific mechanism responsible for the eastward propagation in Hao et al. (1993). Instead, the central Pacific temperature lags behind that of the eastern Pacific, indicating a westward propagation (Fig. 11). This, however, does not affect the basic oscillatory mechanism in this fast-wave limit.

Denote the first and second terms in (27) and (28) as DO and DU (corresponding to SST damping due to Newtonian cooling and upwelling, respectively), and the third term as HU, representing the effect of the thermocline depth on the upwelling. At the peak time, $\partial_t T_e = 0$, which implies that DO and DU balance HU. Figure 11 shows the three terms in the SST equation for the eastern box. The HU, which contributes to the growth tendency, is affected strongly and positively (through a seasonal varying coupling strength) by T_e and weakly and negatively (with a constant coupling strength) by T_c (see B13). During the first 6 months of year -1 prior to the peak time, HU is growing since it is affected mainly by the rapidly growing T_e, which is amplified by a growing coupling strength, whereas the negative effect of T_c is weak due to the small amplitude of the central Pacific warming. Around July, HU reaches its peak due to the combination of the growing T_c and the decreasing coupling strength that weakens the effect of T_e. The SST reaches its peak 2–3 months after the time of maximum HU due to the finite SST adjustment time (i.e., the upwelling timescale). Figure 11 shows that T_e always lags HU by 2 months.

In the fast-wave limit, the mechanism both for the oscillatory nature of El Niño and for the interaction with the seasonal cycle are entirely different from those for the mixed-mode and the fast-SST regimes. The locking of the event's peak time to the seasonal cycle is very different from the observed one. There is only 2–3 months difference between the time of maximum ocean–atmosphere coupling strength and the time of event peaks in the fast-wave regime. Clearly, the additional time delay needed for the events to peak toward the end of the year must come from the finite-wave propagation time, which is omitted in this regime.

5. Seasonal ocean–atmosphere interaction in the CZ model

Throughout this paper we use a linear relation for the coupling between wind stress and SST anomalies (13)

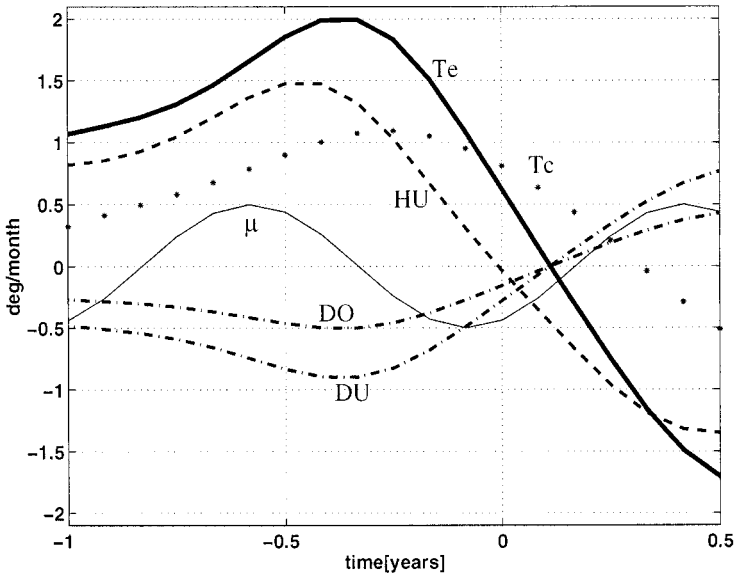

FIG. 11. A time series of the terms in the SST equation for the eastern box in the fast-wave limit for one specific event. The curve DO is the thermal damping term, DU is the damping due to the upwelling, and HU is the part of the upwelling that depends on the thermocline depth h_e.

with a coupling coefficient that varies monthly. We now analyze this seasonal relation using the CZ model. A similar analysis based on observations would have made a stronger point, but such an analysis is left for future work.

The SST and the wind stress anomalies in the CZ model have been least square fitted as $\tau_c^{m,j} = b_0^m \text{Nino3}^{m,j}$, for a 300-yr time series. Here, τ_c is the zonal wind stress averaged over the central Pacific (3°S–3°N and 160°E–120°W), Nino3 is the SST averaged over 5°S–5°N and 90°–150°W, j sums over all the time series points in a given month, and m stands for the month index. Figures 12 and 13 show b_0 as a function of month. There is an evident seasonal cycle with the maximum coupling in May and the minimum coupling in September. Vertical bars indicate the standard deviation of the least squares fit calculation [std(m)], estimated as

$$\text{std}(m) = \sqrt{\sum_{j=1}^{300} (\tau_c^{m,j} - b_0^m \text{Nino3}^{m,j})^2 \Big/ \sum_{j=1}^{300} (\text{Nino3}^{m,j})^2}, \tag{29}$$

where b_0^m is the monthly coupling coefficient calculated from the least square fit, and the summation is over 300 occurrences of each month in the dataset. Clearly std(m), representing the year to year variations in the seasonal coupling, should be small if our phase locking mechanism, which depends on the seasonal variations of b_0, is to account for the fairly robust phase locking in the CZ model. Indeed, it seems that the standard deviation is smaller than the seasonal signal in the coupling coefficient b_0^m.

Based on the dependency of b_0^m on the month of the year, we constructed the simple parameterization for the seasonal variation of the coupling coefficient (16) to reach its maximum in May and its minimum in November. Note again that the behavior of b_0^m was shown by Tziperman et al. (1997) to be mostly a result of seasonal variations in the mean wind convergence and the mean SST.

6. Conclusions

The phase locking of idealized ENSO models to the seasonal cycle was examined in three parameter regimes: the fast-SST limit, the fast-wave limit, and the mixed-mode regime (Neelin 1991; JN93). The idealized models used here for all three regimes are based on simplifications to the dynamics and thermodynamics of the CZ model.

The phase locking mechanism in the mixed-mode and fast-SST regimes relies on the seasonal excitation of the Kelvin and the Rossby waves by wind stress anomalies in the central Pacific basin. The peak time of the events is set by the dynamics to allow a balance between the warming and cooling trends due to downwelling Kelvin and upwelling Rossby waves. This balance is obtained because the warming trend due to the large-amplitude Kelvin waves, amplified by a weak boreal wintertime ocean–atmosphere coupling strength, balances the cooling trend due to weak Rossby waves, amplified by a strong boreal summertime coupling strength. The comparison of ENSO's phase locking in the fast-SST limit and in the mixed-mode regime demonstrated that the

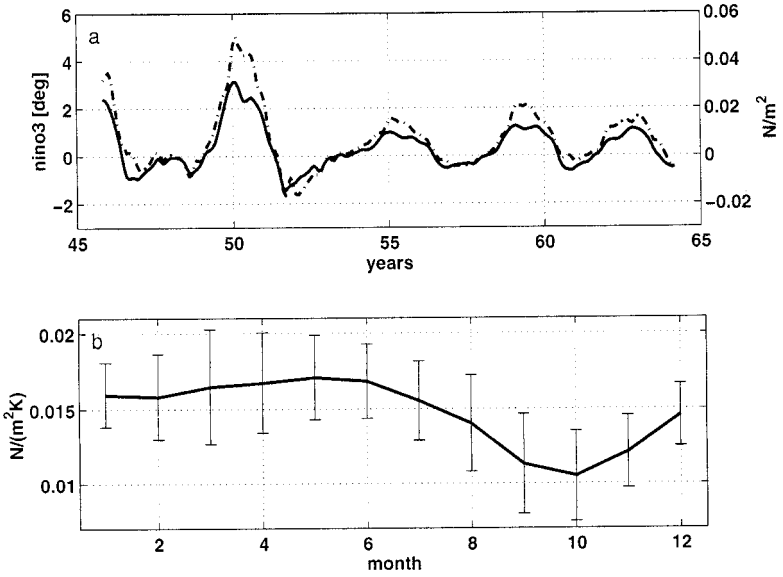

FIG. 12. (a) Time series of Niño-3 (solid) and wind stress τ_c (dash-dot). (b) Regression of τ_c and Niño-3 in the CZ model, as function of month of the year. Vertical bars indicate the variance in the least squares fit.

adjustment time of SST to changes in thermocline depth can shift the event peak time by about 2 months in our idealized models. This SST adjustment time may therefore be an important part of the mechanism responsible for the phase locking of observed ENSO events.

In addition to exploring the detailed locking mechanism, we have shown explicitly that ENSO's phase locking in our simple models is not a result of the model nonlinearity but is a result of the seasonal modulation of the background model parameters and can occur in linearized dynamics as well as in nonlinear dynamics.

In order to support our idealized model analysis, we calculated the seasonal ocean–atmosphere coupling strength (the regression coefficient between the wind stress and the SST) in the CZ model. We showed that the maximum coupling strength occurs in May whereas its minimum is in September, consistent with the coefficient used in the above idealized models.

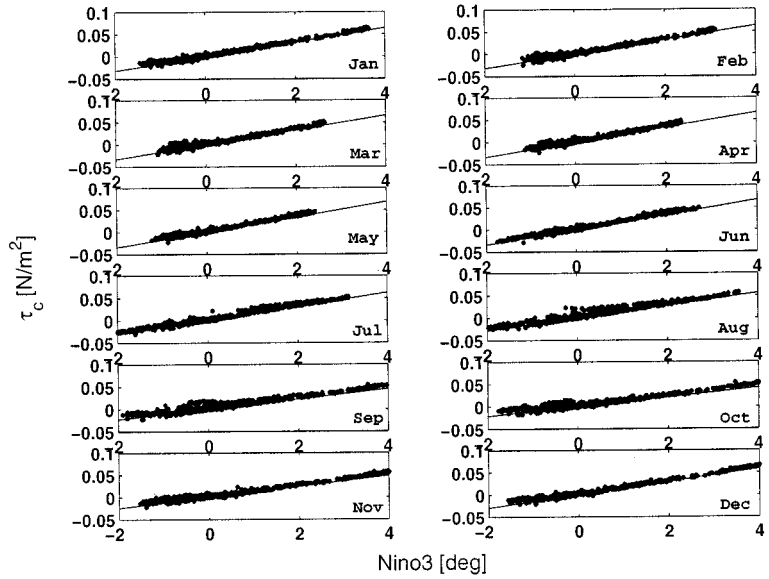

FIG. 13. τ_c vs Niño-3 as function of month of the year. Lines indicate least squares fit.

This study of ENSO's seasonal phase locking mechanism is, hopefully, a step forward from the heuristic model of Tziperman et al. (1998). The simple, yet more rigorously derived models used here enabled us to explore the physical mechanisms underlying ENSO's phase locking to the seasonal cycle in a variety of both more and less realistic parameter regimes. Yet, further validation of the proposed mechanisms, especially by means of data analysis and data assimilation into fuller coupled models, is obviously still needed for a fuller understanding of ENSO's phase locking.

Acknowledgments. We would like to thank Steve Zebiak and Mark Cane for allowing the use of their model and to Yochanan Kushnir for useful discussions. This work was partially funded by the U.S.–Israel Binational Science Foundation.

APPENDIX A

T_{sub} Function

The function that relates deep-temperature anomalies to the deviation of the thermocline from its mean state is taken to be a modified hyperbolic tangent as in Eqs. (9), (10), and (11) of Munnich et al. (1991), yet fitted to the form of T_{sub} in the CZ model:

$$T_{\text{sub}}(h) = \begin{cases} b_+ + \dfrac{b_+}{a_+}\left\{\tanh\left[\dfrac{a_+}{b_+}(h^* - h_+)\right] - 1\right\} \\ \qquad \text{for } h^* > h_+ \\ h^* \quad \text{for } h_- < h^* < h_+ \\ -b_- + \dfrac{b_-}{a_-}\left\{\tanh\left[\dfrac{a_-}{b_-}(h^* - h_-)\right] + 1\right\} \\ \qquad \text{for } h^* < h_-, \end{cases} \tag{A1}$$

where $h_+ = b_+(a_+ - 1)/a_+$; $h_- = -b_-(a_- - 1)/a_-$; $h^* = \kappa h$. We also set

$$\begin{aligned} \kappa &= 0.5\left[\frac{b_1 T_1}{\cosh(b_1\overline{H})^2} - \frac{b_2 T_2}{\cosh(b_2\overline{H})^2}\right], \\ b_+ &= T_1[1 - \tanh(b_1\overline{H})], \\ b_- &= T_2[1 - \tanh(b_2\overline{H})], \end{aligned} \tag{A2}$$

where $T_1 = 28°\text{C}$, $T_2 = -40°\text{C}$, $b_1 = (80\text{ m})^{-1}$, and $b_2 = (33\text{ m})^{-1}$. This parameterization of $T_{\text{sub}}(h)$ provides a close approximation to the form used in the CZ model yet is continuous and has a continuous derivative with respect to h.

APPENDIX B

Derivation of the Fast-Wave Model

The fast-wave limit neglects the time derivative terms in the ocean momentum equations (1). Our derivation of the fast-wave model starts with the equations for the eastward propagating case of Hao et al. (1993). The relation between the wind stress and the SST is as in (11), where $A(T, x)$ is the solution to the Gill-type atmospheric model (Gill 1980), retaining the Kelvin and first Rossby atmospheric modes (Hao et al. 1993),

$$A(T, x) = \frac{1}{2}b_0\epsilon_a\left[3e^{3\epsilon_a x}\int_x^{x_e} T(s)e^{-3\epsilon_a s}\,ds - e^{-\epsilon_a x}\int_{x_W}^{x} T(s)e^{\epsilon_a s}\,ds\right], \tag{B1}$$

where ϵ_a is the nondimensional atmospheric damping. The east–west thermocline tilt in the fast-wave limit is taken to be in balance with the wind stress,

$$C_o^2\rho\partial_x h(x) = \tau(x), \tag{B2}$$

so that

$$h(x) = h_e - \frac{1}{C_o^2\rho}\int_x^{x_E}\tau(s)\,ds. \tag{B3}$$

Following Cane et al. (1991) and Hao et al. (1993), the response of the thermocline at the eastern boundary to wind stress of the form of (11) is taken to be

$$h_e = \frac{1}{C_o^2\rho}\int_{x_W}^{x_E}\tau(s)\left(\frac{s}{L}\right)^{1/2}ds. \tag{B4}$$

In Hao et al. (1993), the SST equation includes the effects of upwelling, meridional advection, and thermal damping. Furthermore, T_{sub} was used there as a total deep temperature rather than a deep-temperature anomaly. We have verified that the nature of the oscillations does not change when the meridional advection term is neglected, the model is changed to an anomaly model, and the mean annual upwelling (which appears in the thermodynamic equation) is taken to be constant throughout the basin. Therefore, we take the thermodynamic equation to be (10), where T_{sub} is modified from Munnich et al. (1991) as given in (A1).

We divide the basin into two zonal boxes (eastern and central Pacific) for temperature, wind stress, and thermocline depth, (T_e, τ_e, h_e) and (T_c, τ_c, h_c), respectively. Equation (B1) is solved for T_c and T_e to give

$$\tau_c = \frac{1}{2}\mu_1 b_0[B_1 T_c + B_2 T_e], \tag{B5}$$

$$\tau_e = \frac{1}{2}\mu_2 b_0[D_1 T_c + D_2 T_e], \tag{B6}$$

$$\begin{aligned} B_1 &= -e^{3\epsilon_a x_c}(e^{-3\epsilon_a x_0} - e^{-3\epsilon_a x_c}) - e^{-\epsilon_a x_c}(e^{\epsilon_a x_c} - 1), \\ B_2 &= -e^{3\epsilon_a x_c}(e^{-3\epsilon_a} - e^{-3\epsilon_a x_0}), \\ D_1 &= -e^{\epsilon_a x_e}(e^{\epsilon_a x_0} - 1), \quad \text{and} \\ D_2 &= -e^{3\epsilon_a x_e}(e^{-3\epsilon_a} - e^{-3\epsilon_a x_e}) \\ &\quad - e^{-\epsilon_a x_e}(e^{\epsilon_a x_e} - e^{\epsilon_a x_0}), \end{aligned} \tag{B7}$$

where μ_1 and μ_2 represent the seasonal background in the central and eastern boxes, respectively; x_0 is the boundary between the two boxes; x_c is the longitude where τ_c and h_c are evaluated; and x_e is the longitude where τ_e and h_e are evaluated. Equations (B3) and (B4) are then solved for τ_c and τ_e to give

$$h_e = \frac{1}{C_o^2\rho}(x_0^2\tau_c + (1 - x_0)^2\tau_e), \tag{B8}$$

$$h_c = h_e - \frac{1}{C_o^2\rho}((x_0 - x_c)\tau_c + (1 - x_0)\tau_e). \tag{B9}$$

Using (B5) and (B6) in (B8) and (B9), respectively, we get

$$h_c = h_c(T_c, T_e), \qquad h_e = h_e(T_c, T_e). \tag{B10}$$

Substituting the above result into (10), we get

$$\partial_t T_c = -\epsilon_T T_c - \gamma\frac{\overline{w}}{H_1}T_c + \gamma\frac{\overline{w}}{H_1}T_{\text{sub}}(h_c(T_c, T_e)), \tag{B11}$$

$$\partial_t T_e = -\epsilon_T T_e - \gamma\frac{\overline{w}}{H_1}T_e + \gamma\frac{\overline{w}}{H_1}T_{\text{sub}}(h_e(T_c, T_e)), \tag{B12}$$

which form our simplified fast-wave model. Table 2 summarizes the model parameters used.

Using those parameters and assuming seasonal variations only for the terms that involve T_e (see section 4b), (B10) takes the form

$$h_c \propto \frac{7}{4}T_c + \mu T_e, \qquad h_e \propto -\frac{4}{5}T_c + \mu T_e, \tag{B13}$$

so that h_c depends positively on T_c and T_e, whereas h_e depends negatively on T_c and positively on T_e.

REFERENCES

Battisti, D. S., 1988: The dynamics and thermodynamics of a warming event in a coupled tropical atmosphere–ocean model. *J. Atmos. Sci.,* **45,** 2889–2919.

——, and A. C. Hirst, 1989: Interannual variability in a tropical atmosphere–ocean model: Influence of the basic state, ocean geometry and nonlinearity. *J. Atmos. Sci.,* **46,** 1687–1712.

Cane, M. A., M. Munnich, and S. E. Zebiak, 1990: A study of self-excited oscillations of the tropical ocean–atmosphere system. Part I: Linear analysis. *J. Atmos. Sci.,* **47,** 1562–1577.

Chang, P., L. Ji, B. Wang, and T. Li, 1995: Interactions between the seasonal cycle and El Niño–Southern Oscillation in an intermediate coupled ocean–atmosphere model. *J. Atmos. Sci.,* **52,** 2353–2372.

Gill, A. E., 1980: Some simple solutions for heat-induced tropical circulation. *Quart. J. Roy. Meteor. Soc.,* **106,** 447–462.

Hao, Z., J. D. Neelin, and F.-F. Jin, 1993: Nonlinear tropical air–sea interaction in the fast-wave limit. *J. Climate,* **6,** 1523–1544.

Hirst, A. C., 1986: Unstable and damped equatorial modes in simple coupled ocean–atmosphere models. *J. Atmos. Sci.,* **43,** 606–630.

Jin, F.-F., 1997a: An equatorial ocean recharge paradigm for ENSO. Part I: Conceptual model. *J. Atmos. Sci.,* **54,** 811–829.

——, 1997b: An equatorial ocean recharge paradigm for ENSO. Part II: A stripped-down coupled model. *J. Atmos. Sci.,* **54,** 830–847.

——, and J. D. Neelin, 1993a: Modes of interannual tropical ocean–atmosphere interaction—A unified view. Part I: Numerical results. *J. Atmos. Sci.,* **50,** 3477–3503.

——, and ——, 1993b: Modes of interannual tropical ocean–atmosphere interaction—A unified view. Part III: Analytical results in fully coupled cases. *J. Atmos. Sci.,* **50,** 3523–3540.

——, ——, and M. Ghil, 1994: ENSO on the devil's staircase. *Science,* **264,** 70–72.

Li, T., 1997: Phase transition of the El Niño–Southern Oscillation: A stationary SST mode. *J. Atmos. Sci.,* **54,** 2872–2887.

Munnich, M., M. A. Cane, and S. E. Zebiak, 1991: A study of self-excited oscillations of the tropical ocean–atmosphere system. Part II: Nonlinear cases. *J. Atmos. Sci.,* **48,** 1238–1248.

Neelin, J. D., 1991: The slow sea surface temperature mode and the fast-wave limit: Analytic theory for tropical interannual oscillations and experiments in a hybrid coupled model. *J. Atmos. Sci.,* **48,** 584–606.

——, and F.-F. Jin, 1993: Modes of interannual tropical ocean–atmosphere interaction—A unified view. Part II: Analytical results in the weak-coupling limit. *J. Atmos. Sci.,* **50,** 3504–3522.

——, D. S. Battisti, A. C. Hirst, F.-F. Jin, Y. Wakata, T. Yamagata, and S. Zebiak, 1998: ENSO theory. *J. Geophys. Res.,* **103** (C7), 14 261–14 290.

Numerical Algorithms Group, 1994: Fortran library manual, mark 16. 6 vols. NAG Ltd. [Available from NAG Wilkinson House, Jordan Hill Road, Oxford OX2 8DR, United Kingdom.]

Philander, S. G., 1983: El Niño Southern Oscillation phenomena. *Nature,* **302,** 295–301.

Picaut, J., F. Masia, and Y. du Penhoat, 1997: An advective–reflective conceptual model for the oscillatory nature of the ENSO. *Science,* **277,** 663–666.

Rasmusson, E., and T. Carpenter, 1982: Variations in tropical sea surface temperature and surface wind fields associated with the Southern Oscillation/El Niño. *Mon. Wea. Rev.,* **110,** 354–384.

Suarez, M. J., and P. S. Schopf, 1988: A delayed action oscillator for ENSO. *J. Atmos. Sci.,* **45,** 3283–3287.

Tziperman, E., L. Stone, M. Cane, and H. Jarosh, 1994: El Niño chaos: Overlapping of resonances between the seasonal cycle and the Pacific ocean–atmosphere oscillator. *Science,* **264,** 72–74.

——, M. A. Cane, and S. Zebiak, 1995: Irregularity and locking to the seasonal cycle in an ENSO prediction model as explained by the quasi-periodicity route to chaos. *J. Atmos. Sci.,* **52,** 293–306.

——, S. Zebiak, and M. A. Cane, 1997: Mechanisms of seasonal–ENSO interaction. *J. Atmos. Sci.,* **54,** 61–71.

——, M. A. Cane, S. Zebiak, Y. Xue, and B. Blumenthal, 1998: Locking of El Niño's peak time to the end of the calendar year in the delayed oscillator picture of ENSO. *J. Climate,* **11,** 2191–2199.

Zebiak, S. E., and M. Cane, 1987: A model El Niño–Southern Oscillation. *Mon. Wea. Rev.,* **115,** 2262–2278.